Long-term change of the Pacific North Equatorial Current bifurcation in SODA

Zhaohui Chen[1] and Lixin Wu[1]

Received 7 December 2011; revised 27 April 2012; accepted 27 April 2012; published 21 June 2012.

[1] The long-term change of the North Equatorial Current (NEC) bifurcation in the Pacific Ocean is assessed based on the recently developed Simple Ocean Data Assimilation (SODA, version 2.2.4). It is found that the NEC bifurcation latitude (NBL) has shifted southward over the past 60 years, although it displayed a slight northward migration from 1970 to 1992. This southward shift of the bifurcation latitude is associated with changes in the wind stress curl over the tropical Pacific Ocean between 10°N and 20°N, leading to the strengthening of the Kuroshio at its origin. The conclusion is further supported by simulations of Intergovernmental Panel on Climate Change models. It is demonstrated that the long-term change of the seasonal south–north migration of the bifurcation is modulated by the southward shift of the mean position. Over the past 6 decades, the phase speed of first-mode baroclinic Rossby waves (C_R) at the latitude of the bifurcation increases from 13 cm s^{-1} in 1950 to 18 cm s^{-1} in 2005, and the corresponding seasonal amplitude increases (decreases) before (after) the mid-1980s. Using a linear vorticity model, it is found that the long-term modulation of the NBL seasonal migration amplitude is associated with the increase of C_R in responses to the southward shift of the mean NBL. It is expected that the seasonal amplitude will decrease moderately in the following decades if the ocean continues warming.

Citation: Chen, Z., and L. Wu (2012), Long-term change of the Pacific North Equatorial Current bifurcation in SODA, *J. Geophys. Res.*, *117*, C06016, doi:10.1029/2011JC007814.

1. Introduction

[2] Over recent years much attention has been paid to the response of wind driven ocean circulation to global warming in the Pacific Ocean [e.g., *Cai et al.*, 2005; *Saenko et al.*, 2005; *Sakamoto et al.*, 2005]. To date, the main focus has been on the behavior of the Kuroshio and the Kuroshio Extension, which connects the subtropical gyre and the subpolar gyre in the North Pacific, as well as the southern midlatitude ocean circulation associated with the change in the wind stress under the scenario of increasing greenhouse gases and global warming. However, little attention has been paid to the low-latitude ocean circulation response to such a warming pattern. Recently, there have been studies addressing the impacts of global warming on the subtropical cells (STC) [*McCreary and Lu*, 1994; *Liu et al.*, 1994] that connect the subtropics with the tropics in the Pacific [e.g., *Merryfield and Boer*, 2005; *Lohmann and Latif*, 2005; *Hazeleger*, 2005; *Wu and Li*, 2007]. The water masses are subducted into the thermocline and carried westward by the North Equatorial Current (NEC), reaching the equator via the western boundary current that is believed to be an important branch of the subtropical-tropical exchanges. So the long-term change of the western boundary current associated with the NEC bifurcation should be extensively studied.

[3] The NEC bifurcates as it encounters the Philippine coast, separating into the northward flowing Kuroshio and southward flowing Mindanao Current (MC) [*Nitani*, 1972]. This partitioning of the trade wind driven flow and its variability along the Philippine coast are of vital importance, not only in determining the meridional heat and water mass exchanges which can regulate the warm pool and East Asian climate, but also to the regional biological processes and to fisheries' management in the western Pacific Ocean [*Lukas et al.*, 1991; *Fine et al.*, 1994; *Kimura et al.*, 2001]. Although studies into the dynamics of the NEC bifurcation latitude (NBL) off the Philippines coast from seasonal to interannual time scales have been intensively carried out by both observational [*Toole et al.*, 1990; *Qu and Lukas*, 2003; *Qiu and Chen*, 2010] and modeling approaches [*Qiu and Lukas*, 1996; *Kim et al.*, 2004; *Chen and Wu*, 2011; *Jensen*, 2011], the long-term change of the NEC bifurcation remains poorly understood due to lack of long-term observations.

[4] In this study, we assess the long-term change of the NEC bifurcation based on a recently developed twentieth century ocean reanalysis product: Simple Ocean Data Assimilation (SODA, version 2.2.4) [*Carton and Giese*, 2008; *Giese and Ray*, 2011]. It is found that the bifurcation

[1]Physical Oceanography Laboratory, Ocean University of China, Qingdao, China.

Corresponding author: Z. Chen, Physical Oceanography Laboratory, Ocean University of China, 238 Songling Rd., Qingdao 266100, China. (chenzhaohui@ouc.edu.cn)

0148-0227/12/2011JC007814

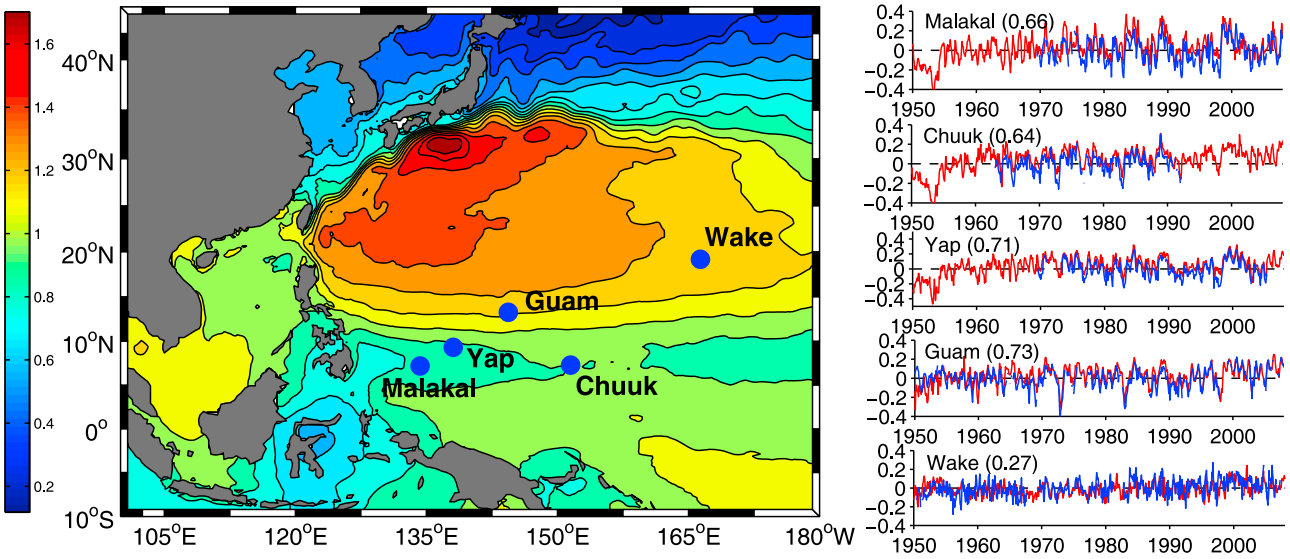

Figure 1. (left) Mean sea surface height field (m) of the western Pacific Ocean from *Rio et al.* [2009]. The blue dots denote locations of the selected tidal gauge stations east of Philippines. (right) The monthly sea level anomaly derived from tide gauges (blue line) and from the gridded sea surface height (SSH) data of Simple Ocean Data Assimilation (SODA) nearest to the tidal gauge stations (red line).

latitude has shifted southward over the past 60 years, although it displayed a slight northward migration from 1970 to 1992. This southward shift of the bifurcation latitude will lead to the strengthening of the Kuroshio at its origin and exert a greater impact on the regional circulation at the low-latitude western Pacific.

[5] This paper is organized as follows: section 2 assesses the performance of the new SODA product in the western Pacific and presents the variability of mean position of the NBL during the past six decades; in section 3, mechanisms controlling the long-term change of the NBL are studied. The long-term change of the NBL seasonal south–north migration will be illustrated in section 4, followed by some discussions and the summary in section 5.

2. Long-Term Change of the NBL

2.1. Performance of New SODA Product

[6] Given the lack of direct long-term observations in the western Pacific, the new version of Simple Ocean Data Assimilation spanning from 1871 to 2008 is employed to assess the long-term change of the NBL.

[7] For the ocean model, the relevant configurations and the assimilation algorithm, the readers are referred to the detailed report on the SODA product [*Carton and Giese*, 2008]. It is worth mentioning that in this version the ocean model is forced by the 20th Century Atmospheric Reanalysis product, designated as 20CRv2 [*Compo et al.*, 2011], which contains the synoptic-observation-based estimate of global tropospheric variability spanning 1871 to 2008 at 6 hourly temporal and 2° spatial resolutions, and is derived using observations of synoptic surface pressure and prescribing monthly SST and sea ice distributions as boundary conditions for the atmosphere.

[8] The sea level is calculated prognostically using a linearized continuity equation with no tidal gauge data assimilated into the model, so the performance of the SODA product in reproducing the long-term change of the sea level could be validated by comparing with tidal gauge data in the western Pacific Ocean. Five tidal gauges in the western Pacific Ocean are selected, among which, Wake/Yap is located at the northern/southern flank of the westward flowing NEC, Guam in the flow axis of the NEC, Malakal located offshore of the Mindanao Current, and Chuuk in the eastward flowing North Equatorial Counter Current (NECC) (see Figure 1 for locations of the tidal gauge stations). Figure 1 shows the time series of the monthly sea level anomalies from the tidal gauges and the Sea Surface Height (SSH) anomalies derived from the SODA product. A good agreement exists between the sea level fluctuations from the tidal gauges and the SODA product on seasonal time scale or longer. The correlation between the time series of the monthly sea level anomalies from the observations and the SODA product are 0.66 (for Malakal), 0.64 (for Chuuk), 0.71 (for Yap), 0.73 (for Guam), and 0.27 (for Wake), respectively. All these values are significant at the 95% confidence level. Generally, the SODA product used here reasonably captures the sea level change in the Northwestern Pacific, which increases our confidence to further assess the long-term change of the NBL. Since the available tidal gauge data can only be tracked back to the middle of the twentieth century, we will only focus on the period 1950 to 2008 in this study.

2.2. Long-Term Change of the NBL in SODA

[9] As demonstrated by *Qu and Lukas* [2003] based on a synthesis of historical hydrological data and *Kim et al.* [2004] using a high-resolution ocean model simulation, the bifurcation occurs at about 15°N for the annual average and is easily identifiable in the upper layer ocean. In this study we define the NBL as a position where the depth-averaged meridional flow in the upper 381 m within 2° band off the Philippine coast is zero. The bifurcation latitude defined by meridional velocity is not sensitive to different averaging longitudes and does not change our conclusions substantially.

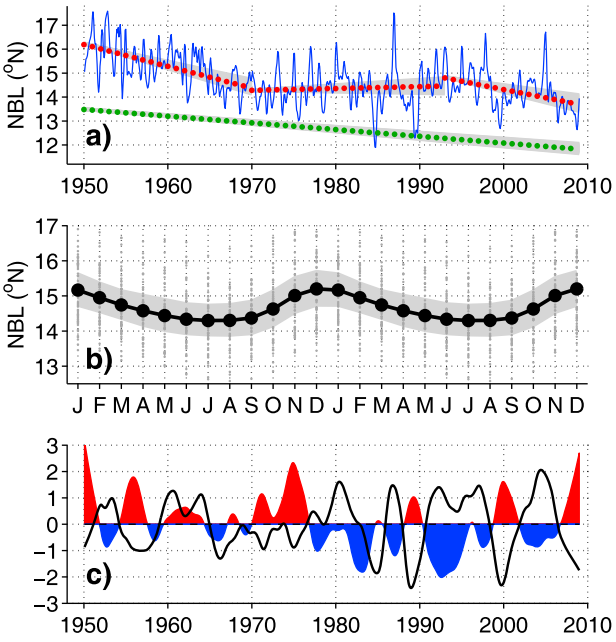

Figure 2. (a) Time series of the North Equatorial Current (NEC) bifurcation latitude (NBL) derived from meridional flow integrated over the upper 381 m (blue line). The red dots indicate the linear trend for the three periods 1950–1969, 1970–1992, and 1993–2008, respectively. The green dots indicate the total linear trend for period 1950–2008. In order not to be mixed up with the linear trend in a different period, the total linear trend is subtracted by 2°. Gray shading indicates the 95% confidence level of the trend. (b) Seasonal variations of the NBL derived from SODA. The gray dots denote individual bifurcation latitude, and the gray shading denotes the standard deviation range. For clarity, the monthly values are plotted for a 2 year time period. (c) Normalized time series of the NBL after the trend is removed (dark line) and Southern Oscillation Index (SOI) (color) after 24.5 month low-pass filtering over the past 60 years.

[10] Figure 2a shows the time series of the monthly NBL derived from SODA. Multiple time scale signals can be detected over the past six decades. For the seasonal variation, the NBL reaches the southernmost latitude in July and the northernmost latitude in December (Figure 2b), consistent with observations and model simulations in the previous studies [*Qu and Lukas*, 2003; *Kim et al.*, 2004; *Wang and Hu*, 2006; *Chen and Wu*, 2011]. The south–north migration of the NBL is about 1° within the range of the observations [*Qu and Lukas*, 2003]. The interannual variability of the NBL that is believed to be associated with the El Niño–Southern Oscillation (ENSO) events [*Qiu and Lukas*, 1996; *Kim et al.*, 2004; *Qiu and Chen*, 2010] is displayed in Figure 2c. The NBL is negatively correlated with the Southern Oscillation Index (SOI), which means the NEC bifurcation occurs at its northernmost position during El Niño years and at its southernmost position during La Niña years. In particular, the anticorrelation between them is more prominent after the 1970s. But during the pre-1970 period, the NBL derived from SODA did not perform well compared with SOI, which implies that the SODA may not be of good quality and this could be attributed to insufficient observational data assimilated into the model. Since our focus is on the long-term change of the NBL, the interannual variability of the NBL will not be discussed in this study.

[11] An apparent feature displayed in Figure 2a is the long-term trend and multidecadal variability of the NBL. Over the past 60 years, the mean position of the NBL has shifted southward from 15.5°N to 13.9°N, at a rate of $-0.028°\ \mathrm{yr}^{-1}$. This type of southward shift in NBL is associated with an equatorward stretching of the boundary between the tropical gyre and the subtropical gyre in the upper western Pacific Ocean. This implies a substantial impact on the origin of the low-latitude western boundary current near the Philippine coast.

[12] It is found that the mean position of the NBL does not progress southward continuously. In addition to the linear trend, multidecadal variability can be identified as well. During the first 20 years, the mean position of the NBL shifts equatorward by over 2°, signifying an expanding subtropical gyre and a shrinking tropical gyre. On the contrary, from 1970 to 1992, the NBL migrates slightly northward by 0.2°. After the early 1990s, the mean position of the bifurcation shifts southward again with the same trend as in the first 20 years, which is consistent with the observational results derived from the 17 year long satellite altimetry data [*Qiu and Chen*, 2010].

[13] In the next section, the controlling dynamics of such a prominent multidecadal variability and linear trend of the NBL over the past six decades will be examined, with special focus on the role of large-scale wind stress forcing.

3. Causes of the Long-Term Change in the NBL

3.1. Role of Large-Scale Wind Stress Forcing-Sverdrup Balance

[14] To demonstrate the relation between the bifurcation latitude in the upper ocean and large scale wind stress curl at decadal time scales, the mean flow, NBL and wind stress curl over three typical decades are calculated. It is shown that the bifurcation latitude of the NEC corresponds pretty well with the zero zonal-integrated wind stress curl line (Figure 3), implying that the NBL is largely governed by the Sverdrup dynamics on decadal or longer time scales.

[15] Given the basin-scale wind stress curl field, the oceanic gyre circulation, as well as the total transport in the interior ocean, can be derived in terms of Sverdrup balance [*Pedlosky*, 1996] as

$$\psi = -\frac{1}{\rho_0 \beta}\int_x^{x_e} \nabla \times \boldsymbol{\tau} dx, \qquad (1)$$

where ψ is the total stream function for flow integrated in the entire water column, β is the meridional derivative of the Coriolis parameter, ρ_0 is the mean density of the seawater, $\nabla \times \boldsymbol{\tau}$ is the wind stress curl, and x_e is the x-coordinate of the eastern boundary. According to equation (1), the NEC should bifurcate along the line of zero zonal-integrated wind stress curl at the latitude where no western boundary current compensates the total interior transport. Although equation (1) represents the total stream function for the entire water column, this model can be applied to the upper ocean's response to the wind forcing by assuming a

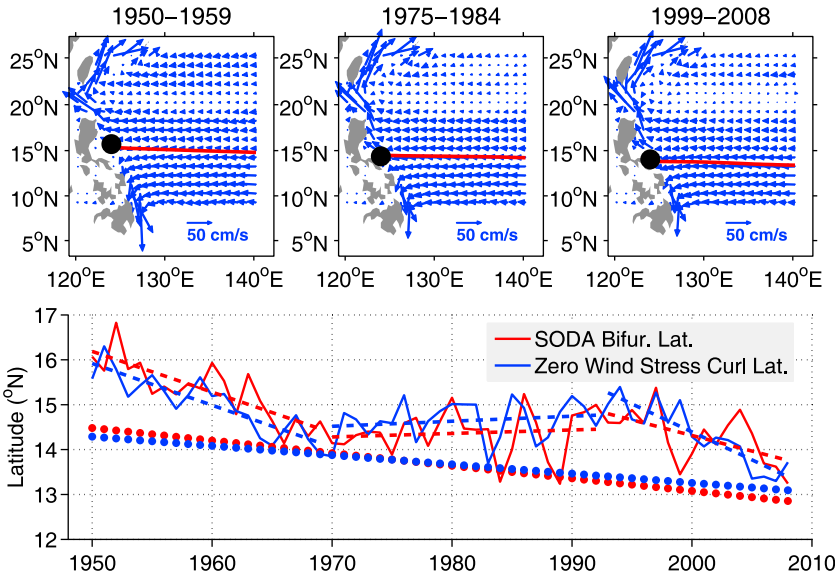

Figure 3. (top) Depth-integrated flow over the upper 381 m (blue vectors) in three typical decades, 1950–1959, 1975–1984, and 1999–2008, derived from the SODA product. The dark dots indicate the position of the NBL, and the red lines indicate zero contour of the wind stress curl integrated from east to west in the corresponding decades. (bottom) Yearly mean NBL derived from SODA (red) and latitude of zero wind stress curl line integrated over the entire ocean (blue). The dashed lines indicate the linear trend for the three periods 1950–1969, 1970–1992, and 1993–2008, respectively. The dots indicate the total linear trend for period 1950–2008. The total linear trend is subtracted by 1° for clarity.

motionless deep interior ocean and that the upper ocean has reached the quasi-equilibrium state at longer time scale.

[16] It is demonstrated that the long-term change of the yearly mean NBL is consistent with the migration of the latitude of zero wind stress curl line integrated from east to west over the Pacific Ocean (Figure 3). Note that even though the annual excursion of the seasonal wind is very large [see *Chen and Wu*, 2011, Figure 5], the baroclinic adjustment effects in the upper ocean would be insignificant at time scales longer than the crossing-basin time of first-mode baroclinic Rossby waves, leaving the low-frequency signals excited by the large scale wind stress. In the North Pacific, the baroclinic long Rossby wave speed C_R ranges from 12 cm s^{-1} in the eastern basin to 20 cm s^{-1} in the western basin [*Chelton et al.*, 1998] at the latitude of the NEC bifurcation, leading to a transit time of 3–4 years which is much shorter than the decadal time scale we are interested in here. Therefore, at decadal or longer time scales, the latitude of the NEC bifurcation could be readily obtained by the wind stress curl field over the Pacific Ocean.

[17] In addition to this long-term trend (the southward shift of the zero line of wind stress curl), multidecadal variability can also be detected in Figure 3. The zero line undergoes a southward shift during 1950–1969, a weak northward migration from 1970 to 1992, and then a southward shift again afterward. This multidecadal variability of the NBL and the corresponding wind stress pattern derived from the 20CRv2 are consistent with recent studies by *Qiu and Chen* [2012]. They demonstrated that changes in the NBL as well as the NEC transport can be understood from the multidecadally modulating surface wind forcing field which is in agreement with the sea level pressure data analysis by *Vecchi et al.* [2006]. They suggested that the easterly trade winds had a decreasing trend over the period 1972–1992, followed by an increasing trend over the 1993–2009 across the tropical Pacific Ocean.

[18] Nevertheless, the multidecadal variations of the NBL cannot be simply attributed to the decreasing/increasing of the trade wind intensity, as suggested in previous studies [*Qiu and Chen*, 2012], since the decreasing trade wind would still produce a negative wind stress curl anomaly over the tropical Pacific Ocean which favors the southward shift of the NBL. It is demonstrated in Figure 4 that the linear trend of the trade wind intensity in the tropical Pacific has indeed weakened over 1970–1992 and strengthened after early 1990s, and the wind stress curl, as a consequence, displays an increasing and a decreasing trend, respectively. If we further examine the trade wind during the period 1950–1969, a weakened trade wind intensity can be found at its northern branch (around 20°N) and this leads to negative wind stress curl anomaly between 10°N and 20°N all the same (Figure 4). Therefore, the multidecadal variation of the NBL associated with the shift of the zero wind stress curl line is attributed to the change in the wind stress curl over the tropical Pacific Ocean between 10°N and 20°N, rather than the intensity of trade wind alone.

[19] The equatorward shift of the zero zonal-integrated wind stress curl line in the tropical Pacific Ocean is also supported by other wind stress products in spite of some notable interdata discrepancies. In addition to the 20CRv2 atmospheric reanalysis, the monthly wind stress data of 1959–2009 from the European Centre for Medium Range Weather Forecasts (ECMWF) Ocean Analysis System ORA-S3 [*Balmaseda et al.*, 2008] and a recently constructed Wave and Anemometer-based Sea-surface Wind data set (1950–2009, WASWind, resolution is 4° by 4°) [*Tokinaga*

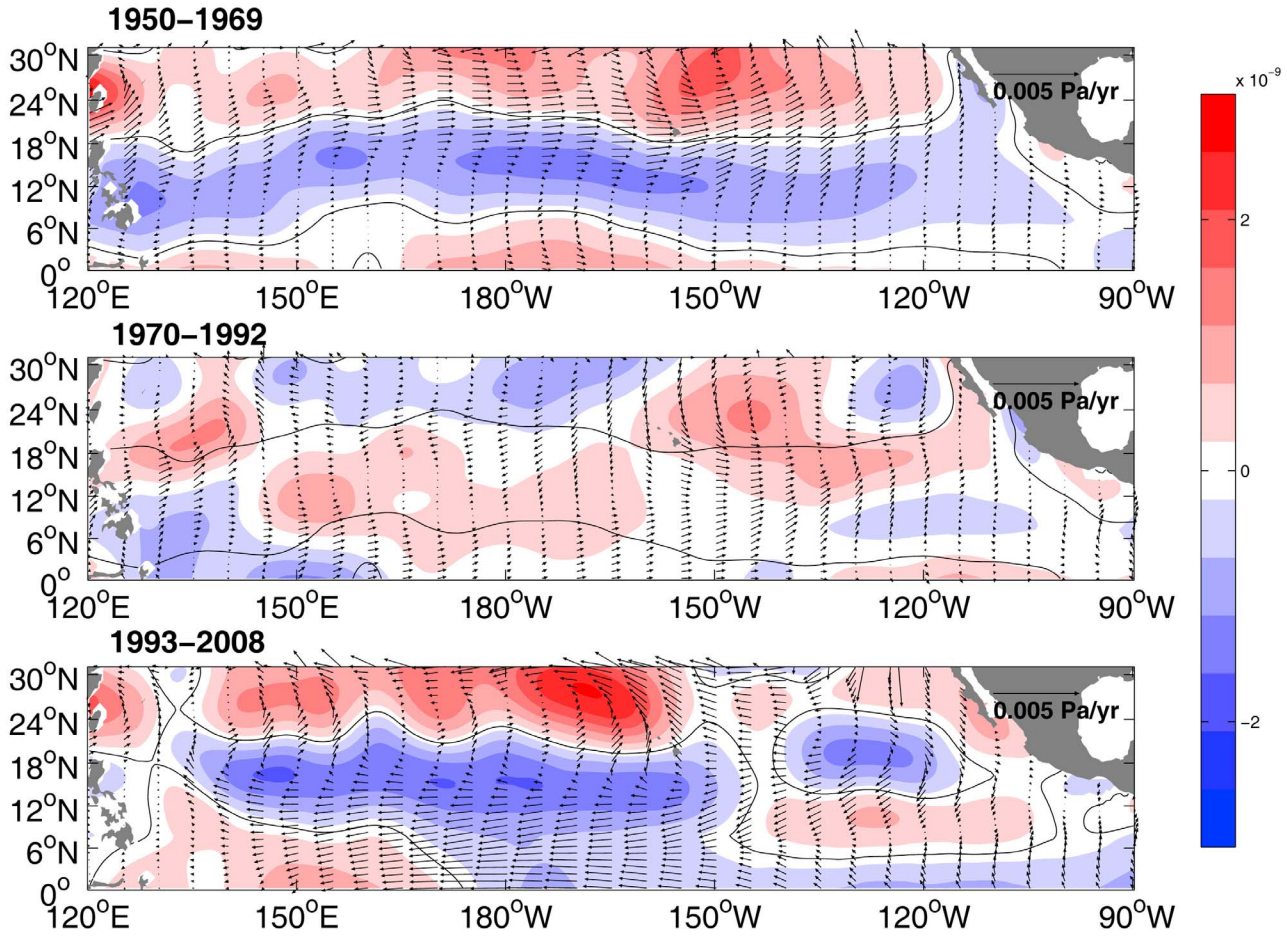

Figure 4. Linear trends in wind stress (vectors) and wind stress curl (color) over the periods of 1950–1969, 1970–1992, and 1993–2008 based on the 20CRv2 atmospheric reanalysis. The unit of the trend in wind stress curl is Pa m^{-1} yr^{-1}.

and Xie, 2011] are used to verify the linear trend as well as the multidecadal transition in the wind stress curl pattern. Over the past half century, all the wind stress curl from these data display negative trends in the tropical Pacific Ocean with the zero lines shifted equatorward. Meanwhile, a weak northward migration over 1970–1992 is also detected in all data sets, indicating the robustness of the multidecadal transition in the wind stress curl pattern over the tropical Pacific Ocean (Figure 5).

3.2. Interior Transport in SODA

[20] It is worth emphasizing that the 60 year long trend and multidecadal variability of the NBL can be physically illustrated in terms of mass conservation. For the long-term change of total mass across a certain latitude, the transport carried by the western boundary current should be equal to the interior transport in the upper ocean. A negative wind stress curl anomaly over the tropical Pacific Ocean generates a southward transport anomaly in the interior and a returning northward flow anomaly in the western boundary current, therefore favoring a southward shift of the NBL (Figures 6a and 6b). However, these linear trends are only confined in the low-latitude Pacific, while they do not increase significantly north of 23°N over the past six decades. Therefore, this conclusion derived from the SODA product cannot be

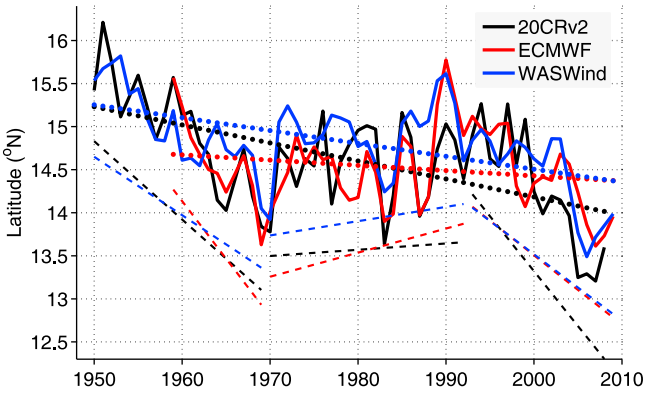

Figure 5. Yearly mean latitude of zero zonal-integrated wind stress curl derived from 20CRv2 (dark), European Centre for Medium Range Weather Forecasts (ECMWF) ORA-S3 (red), and Wave and Anemometer-based Sea-surface Wind (WASWind) (blue). The dots indicate the total linear trend for each wind stress data set, and the linear trends are all over 95% confidence level. The dashed lines indicate the linear trend of each data set for the three periods starting year–1969, 1970–1992, and 1993–ending year, respectively. The part-time linear trend is subtracted by 1° southward for clarity.

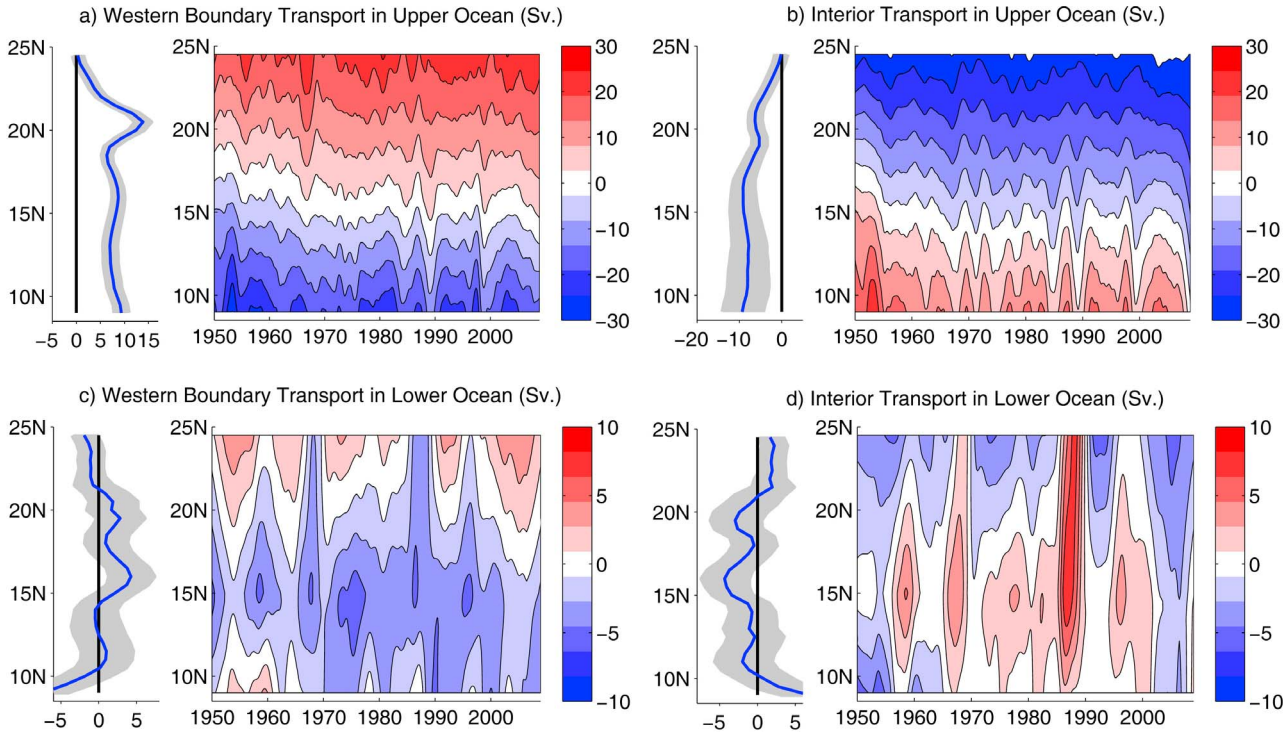

Figure 6. (a) Time-latitude plot of the western boundary transport in the upper ocean. (b) Same as Figure 6a but for the interior transport in the upper ocean. (c) Same as Figure 6a but for the western boundary transport in the lower ocean. (d) Same as Figure 6b but for the interior transport in the lower ocean. The blue lines indicate the linear trend of the transport over the past 60 years. Gray shading indicates the 95% confidence level of the trend.

extended to higher latitude. This is consistent with the observational results that the gyre-scale circulation is limited to south of Luzon Strait over the 1993–2009 period [*Qiu and Chen*, 2012]. If we further examine the lower layer transport, it is interesting that there is no significant trend either at the western boundary or in the interior ocean. So the long-term change of the interior transport in response to the large scale wind stress forcing is confined to the upper layer (Figures 6c and 6d), implying a vital role of the wind stress forcing on the upper ocean circulation in the North Pacific.

[21] Note that the interior transport in the upper ocean consists of two parts: transport in the Ekman layer and geostrophic transport below the Ekman layer. To show more details of their contributions to the interior transport, we plot in Figure 7 the time evolution of each component derived from the SODA product. For simplicity, the Ekman layer depth is set to be spatially uniform (36 m) despite some minor discrepancies from the isopycnal surface and this way of calculation does not change the conclusion substantially.

[22] It is demonstrated in Figure 7a and Figure 7b that both the transport in the Ekman layer and the geostrophic transport present a negative trend over the past six decades, but the decreasing trend of the Ekman component is not as significant as the geostrophic component. This insignificant trend is also verified by calculating the meridional Ekman transport using the 20CRv2 wind stress, although the wind stress derived Ekman transport is larger than the meridional velocity derived transport in the Ekman layer (note that it includes a small quantity of geostrophic component in the Ekman layer) (Figure 7c). Therefore, the long-term change of the southward transport in the interior in the past six decades is mainly caused by the geostrophic component below the Ekman layer and this significant trend can be further diagnosed from the difference of the 20°C isotherm between the western basin and the eastern basin in the tropical Pacific Ocean. With the wind stress curl becoming more negative, the southward transport is enhanced, thus increasing the west–east thermocline slope (Figure 7d).

3.3. Projected NBL Under Global Warming

[23] The trend of southward migration of the NBL over the past six decades may be associated with the warming of the global climate. To test this hypothesis, we examined climate model experiments performed for the Intergovernmental Panel on Climate Change (IPCC) Fourth Assessment Report (AR4). Here we explore climate change simulations from 22 different coupled climate models integrated with 20th Century Climate in Coupled Models (20C3M) and projected changes in well-mixed greenhouse gases and aerosols as prescribed by the IPCC Special Report on Emissions Scenarios (SRES) A1B scenario (SRESA1B) [*Meehl et al.*, 2007]. Both of these two scenarios aim to show the response of the tropical atmospheric and oceanic circulation to increasing greenhouse gases, with special emphasis on the change of the wind stress curl/zero wind curl line over the tropical Pacific Ocean, in order to deduce the change of the NBL. For the SRESA1B experiments, the results of 2000–2100 with progressively increasing greenhouse gases are examined.

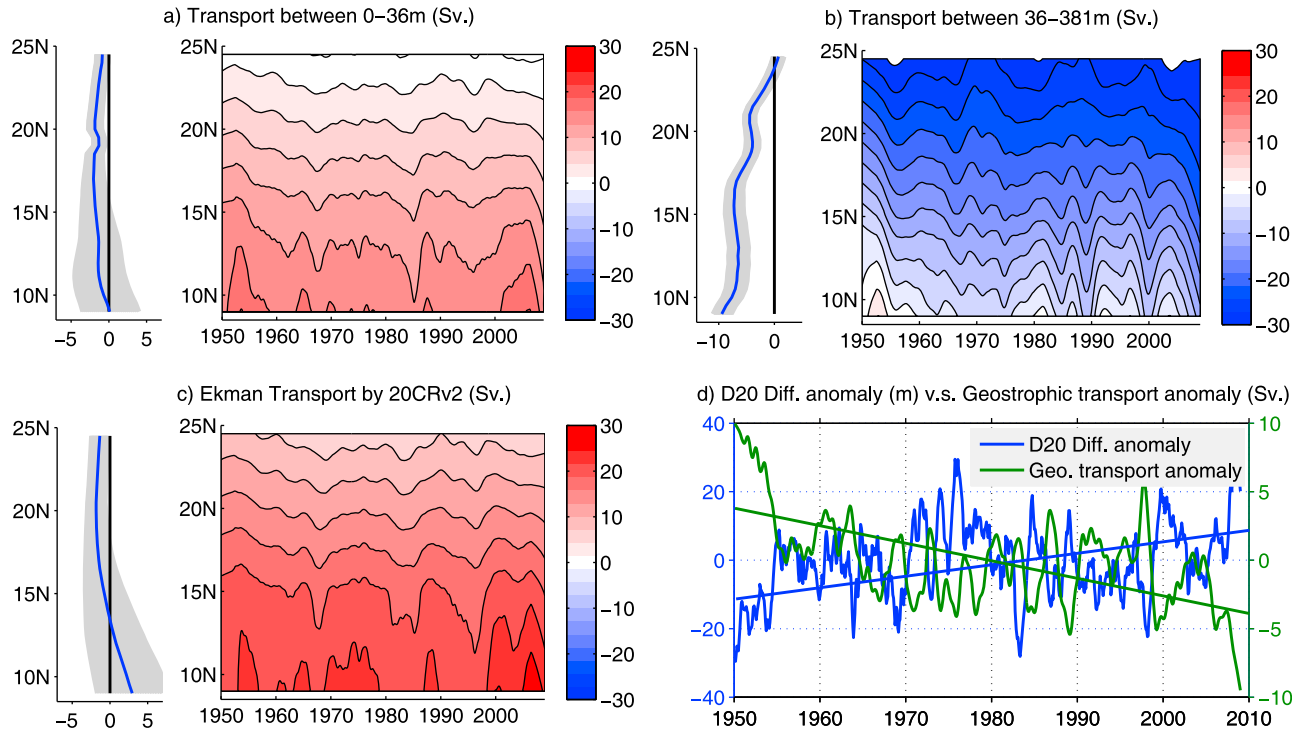

Figure 7. (a) Time-latitude plot of the Ekman layer transport (0–36 m) in the interior ocean. (b) Same as Figure 7a but for the geostrophic transport (36–381 m) in the interior ocean. (c) Same as Figure 7a but for the Ekman transport calculated by the 20CRv2 wind stress. The blue lines indicate the linear trend of the transport over the past 60 years. Gray shading indicates the 95% confidence level of the trend. (d) Depth of 20°C difference anomaly between western basin (130°E–180°E, 10°N–20°N) and eastern basin (160°W–100°W, 10°N–20°N) derived from SODA (blue line) and geostrophic transport anomaly in the ocean interior (130°E–eastern boundary, green line) averaged between 10°N and 20°N derived from SODA. The solid lines denote the linear trend of the time series.

[24] It is demonstrated that two thirds of the models indicate a southward shift in the zero wind stress curl line in both 20C3M and SERSA1B, although the migration is much less than that we have obtained from the 20CRv2 atmospheric reanalysis in the past 60 years (Figure 8). Most of the southward shifts are confined within 0.2° per century, indicating the response of wind in the low-latitude to global warming is less sensitive than that in the mid/high-latitude. The cause of the inconsistency of the latitude of zero wind stress curl line as well as these wind shifts in multiple models may be associated with different responses of tropical ocean and atmosphere circulations to global warming among different models, which is beyond the scope of this paper.

4. Long-Term Change of the NBL Seasonal Amplitude

[25] The NBL displays a distinct seasonal cycle (recall Figure 2b). The seasonal south–north migration of the NEC bifurcation not only determines the seasonal variability of the Kuroshio and Mindanao Current at their origins near the Philippine coast, but also exerts significant impacts on the regional dynamic environment on the seasonal time scale. Furthermore, it is desirable to illustrate the modulation of the low-frequency change (i.e., long-term change of the mean position of the NBL) on high-frequency variability (i.e., seasonal variability of the NBL). In the following section, we will examine in more detail the long-term change of the seasonal amplitude of the NBL (hereinafter A_b) with special focus on the role of oceanic adjustment associated with the baroclinic Rossby waves propagation.

4.1. Performance of the Models

[26] In order to capture the main factors in controlling A_b, we simplify the ocean into an idealized one active layer representing the water above the main thermocline with only the first-mode baroclinic Rossby waves allowed. The water under the thermocline is infinitely deep and motionless. A 1.5 layer nonlinear reduced gravity model and a linear vorticity model are adopted to explore the long-term change of A_b. For more information on the configurations of the numerical model, the readers are referred to *Chen and Wu* [2011]. The linear vorticity model is derived from the primitive equation, which governs the 1.5 layer ocean by adopting the long-wave approximation. The equation can be written in terms of the perturbation thermocline depth h (which can also be regarded as the upper layer thickness) as

$$\frac{\partial h}{\partial t} + C_R \frac{\partial h}{\partial x} = -\frac{1}{\rho_0 f} \nabla \times \boldsymbol{\tau} - \varepsilon h, \tag{2}$$

where C_R is the phase speed of first-mode baroclinic long Rossby waves, f is the Coriolis parameter, ρ_0 is the mean density of the upper layer ocean and ε is the Newtonian

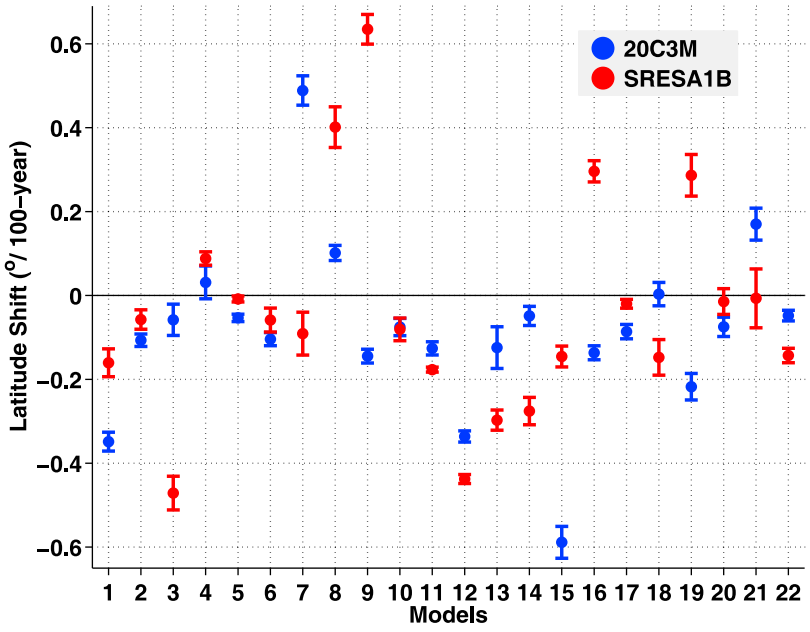

Figure 8. Linear trend of the latitude of zero zonal-integrated wind stress curl derived from 22 coupled climate models (blue for 20C3M and red for SRESA1B). The bar denotes the 95% confidence level for each trend. The models are cccma_cgcm3_1, cccma_cgcm3_1_t63, cnrm_cm3, csiro_mk3_0, csiro_mk3_5, gfdl_cm2_0, gfdl_cm2_1, giss_aom, giss_model_e_h, giss_model_e_r, iap_fgoals1_0_g, ingv_echam4, inmcm3_0, ipsl_cm4, miroc3_2_hires, miroc3_2_medres, miub_echo_g, mpi_echam5, mri_cgcm2_3_2a, ncar_ccsm3, ncar_pcm1, ukmo_hadcm3, and ukmo_hadgem1.

dissipation rate with the unit of year^{-1} (in this study we choose $\varepsilon = 0$ since it does not change the seasonal cycle of the NBL essentially, figure is not shown). Integrating equation (2) along the long Rossby wave characteristic line, we obtain

$$h(x,y,t) = \frac{1}{\rho_0 f}\int_{x_e}^{x} \frac{1}{C_R}\nabla \times \boldsymbol{\tau}\left(x', y, t - \frac{x-x'}{C_R}\right) \times \exp\left[-\frac{\varepsilon(x-x')}{C_R}\right] dx'. \quad (3)$$

In equation (3) we have ignored the solution due to the eastern boundary forcing because its influence is limited to the area hundreds of kilometers away from the eastern boundary [*Fu and Qiu*, 2002; *Cabanes et al.*, 2006]. The wind stress curl used here is derived from the 20CRv2 atmospheric reanalysis monthly data spanning from 1950 to 2008. Following *Qiu and Lukas* [1996], mass conservation requires the inflow at the western boundary to bifurcate where $h = 0$ if the detailed flow structures inside the western boundary are neglected, so we define the NBL in the linear model as the position where mean h within 2° off the western boundary is zero.

[27] It is necessary to check the validity of the present model results prior to analyzing the long-term change of A_b. Figure 9 shows the comparison between the NBL derived

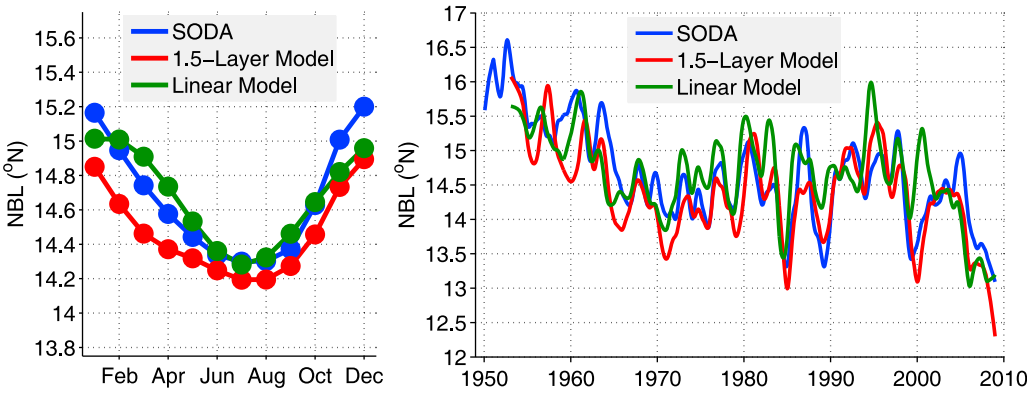

Figure 9. (left) Seasonal cycle of the NBL derived from SODA (blue), 1.5 layer reduced gravity model (red) and linear vorticity model (green). (right) The 24.5 month low-pass filtered NBL by SODA (blue), 1.5 layer reduced gravity model (red), and linear vorticity model (green).

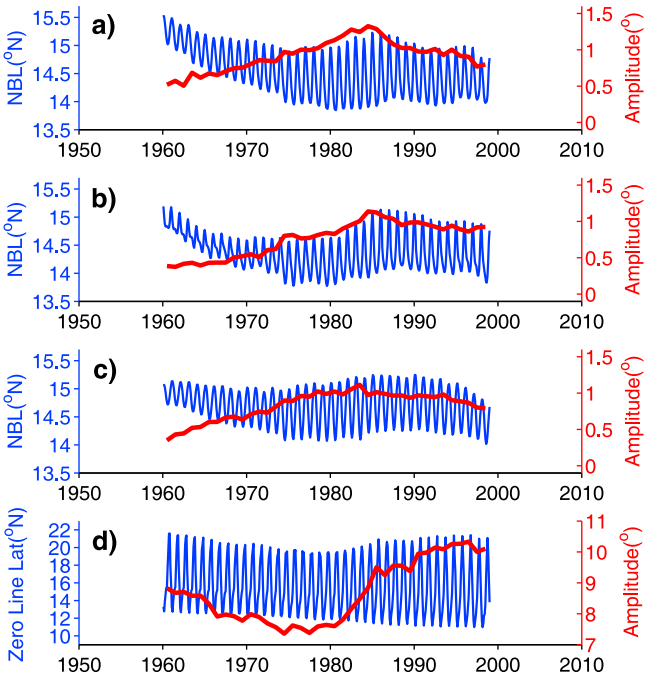

Figure 10. Time series of the NBL/latitude of zero zonal-integrated wind stress curl line with 21 year running mean (blue) and seasonal amplitude (red) derived from (a) SODA, (b) 1.5 layer reduced gravity model, (c) linear vorticity model, and (d) 20CRv2 wind stress data.

from the models and the SODA product. Both of these models reasonably reproduce the seasonal variation of the NBL in peak seasons and amplitude of the south–north migration, as well as the interannual variability compared with SODA product.

4.2. Long-Term Change of A_b

[28] To eliminate the influence from the interannual/decadal variations, a 21 year running mean is conducted to calculate the optimized NBL. Figures 10a–10c show the time series of the optimized NBL and its corresponding A_b. In addition to the southward shift of the mean position, there is a noticeable feature both from SODA and model runs: A_b increases before the mid-1980s and then falls after that, with a magnitude of about 0.5°. As previous studies suggested, the seasonal variations of the bifurcation point is predominantly governed by Rossby wave dynamics in association with both external wind forcing and baroclinic Rossby wave propagations [*Qiu and Lukas*, 1996, 2003; *Chen and Wu*, 2011]. The consistent changes of A_b between SODA and simple models confirm that the long-term change of A_b may be explained simply by oceanic wave dynamics.

[29] To explore the factors in controlling the long-term change of A_b, we first examine the long-term change of the seasonal south–north excursion of the zero wind stress curl line (A_w). It is demonstrated in Figure 10d that the long-term change of A_w does not share the same pattern with A_b, specifically, it decreases before the mid-1970s and then increases after that, with a magnitude of over 2°. The inconsistency between A_w and A_b implies that the internal ocean adjustment would be the primary factor in determining the variations of A_b. A recent work by *Chen and Wu* [2011] has systematically explored the dynamics of the seasonal variation of the NBL and they concluded that A_b is largely sensitive to C_R. Meanwhile, it has been demonstrated in section 2 that the mean position of the NBL has shifted equatorward by over 1.5° and this southward shift would be in favor of a faster adjustment of the upper ocean to the wind forcing over the entire basin around the bifurcation latitude. So it is more straightforward to associate the long-term change of A_b with the increasing C_R. In the following section, we will first examine the long-term change of C_R derived from SODA and from the 1.5 layer reduced gravity model simulation, and then try to use the linear model to test our hypothesis by changing only C_R while the wind stress curl is set to the monthly climatology.

4.3. Role of the Wave Speed

[30] It is shown in Figure 11a that C_R at the latitude of the bifurcation point increases from almost 13 cm s^{-1} in 1950 to 18 cm s^{-1} in 2005 with its linear trend 0.9 cm s^{-1} per decade. This trend is slightly greater than that calculated from the 1.5 layer reduced gravity model simulation. This discrepancy is largely due to the fact that the 1.5 layer reduced gravity model could not capture the effect of warming in the upper ocean, since the increased sea surface temperature over the past 60 years leads to an enhanced stratification and thus the extra increased C_R, while the stratification is constant in the model. This discrepancy, however, is not significant, indicating that the long-term change of C_R is primarily attributed to the southward shift of the mean position.

[31] To explicitly demonstrate the relationship between A_b and C_R, we extend the range of C_R in the linear vorticity model in which the wind stress curl only exhibits the seasonal cycle to assure that the mean position of the NBL is

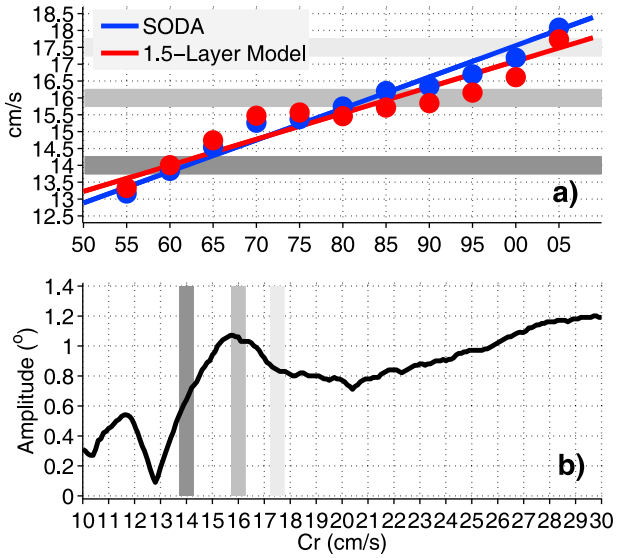

Figure 11. (a) Phase speed of first-mode baroclinic long Rossby waves at the latitude of the NEC bifurcation calculated by the WKB method using temperature and salinity data from SODA product [*Chelton et al.*, 1998] (blue) and by $\beta g'H/f^2$ from the 1.5 layer reduced gravity model (red). (b) Seasonal amplitude as a function of C_R in the linear vorticity model.

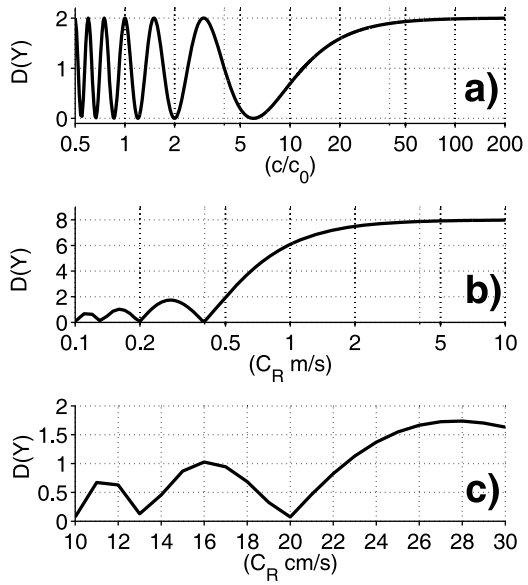

Figure 12. (a) Variance of Y as a function of c/c_0. The logarithm coordinate is used. (b) Variance of Y as a function of C_R. The Logarithm coordinate is used. (c) Same as Figure 12b but for C_R ranges from 10 cm s^{-1} to 30 cm s^{-1}.

unchanged. The wind stress curl used in this sensitivity test is the monthly climatology derived from the 20CRv2 atmospheric reanalysis from 1950 to 2008. Figure 11b shows A_b as a function of C_R obtained by the linear vorticity model. In terms of the linear trend, the amplitude increases along with increasing C_R, consistent with the previous conclusions that there will be less cancellation between local annually reversed wind forcing and the westward propagating anomalies if the Rossby waves travel fast. The linear trend, however, is characterized by significant undulations. As shown in Figure 11b, the amplitude rises as C_R increases from 14 cm s^{-1} to 16 cm s^{-1} and falls as C_R continues increasing from 16 cm s^{-1} to 17.5 cm s^{-1}. It is worth noting that the increasing C_R from 14 cm s^{-1} to 16 cm s^{-1} and from 16 cm s^{-1} to 17.5 cm s^{-1} corresponds to the period 1960–1985 and 1985–2000, during which A_b rises and falls, respectively (recall Figures 10a–10c).

[32] It is interesting that A_b decreases at a certain range of C_R rather than increasing all the time. Consider the simplest case: the NEC bifurcation at the western boundary (WB) is determined by both local forcing and remote forcing. Assume the local forcing is

$$F_{local} = \sin(\omega t), \tag{4}$$

where $\omega = 2\pi/T_0$, and T_0 is the primary period of the forcing. Here we can regard $\sin(\omega t)$ as the zero wind stress curl line with south–north extent of -1 to 1. Meanwhile, the bifurcation is also affected by the remote forcing via baroclinic Rossby waves. For simplicity we just consider one point as the remote forcing, so the impact of the remote forcing on the bifurcation can be expressed as

$$F_{remote} = \sin\left[\omega\left(t - t_{lag}\right)\right], \tag{5}$$

where $t_{lag} = L/c$ is the time lag for signals propagating from *Remote* to *Local*, L is the characteristic length between *Local* and *Remote* and c is the wave speed. The final response to the forcing can be written as $Y(t) = \sin(\omega t) + \sin[\omega(t–L/c)]$. We simplify $Y(t)$ to

$$Y(t) = 2\sin\left(\omega t - \frac{\omega L}{2c}\right)\cos\left(\frac{\omega L}{2c}\right), \tag{6}$$

so the seasonal amplitude of the NEC bifurcation can be represented by its variance $D(Y)$ as

$$D(Y) = 1 + \cos\left(\frac{\omega L}{c}\right). \tag{7}$$

Assuming $L = 3T_0c_0$ (consider 3 year transit time), where c_0 is the reference wave speed, so $D(Y)$ can be easily derived by extending c from $0.5c_0$ to $200c_0$. It is obvious in Figure 12a that $D(Y)$ displays wave-like change along with c/c_0, which can be attributed to the phase shift by the varying L/c. In the more realistic case, the bifurcation of the NEC at the WB is determined by N points rather than two points. Here we assume the east–west length is 1.25×10^7 m and there are 100 points with amplitude of ± 4 (consider the 8° south–north migration of the zero wind stress curl line) evenly distributed over the entire ocean. We can obtain the variance $D(Y)$ by extending C_R from 0.01 m s^{-1} to 10 m s^{-1} artificially. It is demonstrated in Figure 12b that $D(Y)$ exhibits not only an increasing/decreasing pattern, but also a distinct linear trend. This pattern resembles the result from the synthetic expression given by *Qiu and Lukas* [1996] pretty well (not shown). However, C_R would not be so large in the real ocean. Within a more realistic range of 10–30 cm s^{-1}, the increasing/decreasing pattern as well as the amplitude is analogous to the results derived from the linear vorticity model (Figure 12c), although the amplitude differs greatly as C_R increases from 18 cm s^{-1} to 20 cm s^{-1}. This may be due to the fact that the sinusoidal model is idealized and simple while in the linear model it is forced by the realistic wind stress which is not spatially uniform.

[33] The experiments by the linear vorticity model and the sinusoidal model above suggest that the increasing/decreasing pattern of A_b before/after the mid-1980s in SODA may be attributed to the increasing C_R, which plays an important role in modulating the south–north migration of the NEC bifurcation.

5. Discussion and Summary

[34] The recently developed twentieth century ocean reanalysis product offers excellent opportunities to study the long-term change of the NEC bifurcation in the Pacific Ocean. Over the past six decades, it has been found that the mean position of the bifurcation latitude shifted southward from 15.5°N to 13.9°N, at a rate of $-0.028°$ yr^{-1}. This southward shift of the bifurcation latitude is largely governed by Sverdrup dynamics and it is associated with the substantial changes in the wind stress curl over the tropical Pacific Ocean between 10°N and 20°N.

[35] In addition to the linear trend, multidecadal variability of the NBL can be identified as well. The mean position of the NBL shifts equatorward from 1950 to the late 1960s

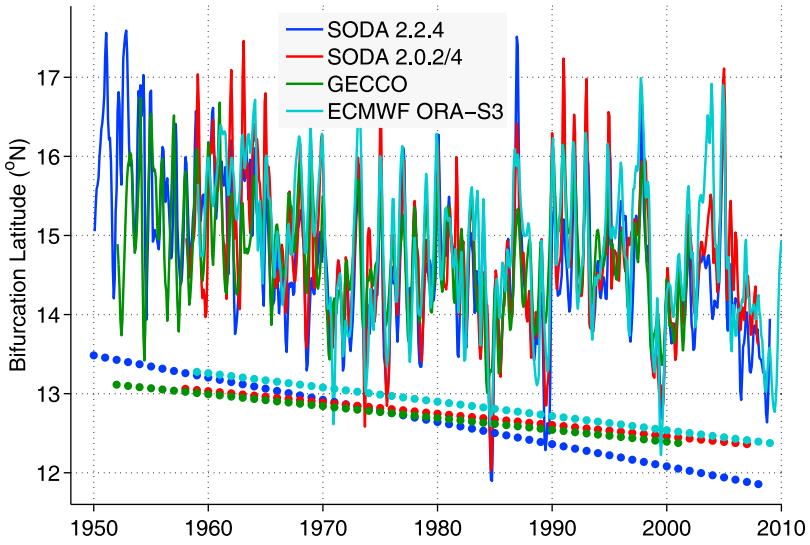

Figure 13. Time series of the NBL derived from multiple reanalysis product (blue line, SODA 2.2.4 upper 381 m; red line, SODA 2.0.2/2.0.4 upper 381 m; green line, GECCO upper 435 m; cyan line, ECMWF ORA-S3 upper 415 m). The dots indicate the linear trend for NBL of each product and are subtracted by 2° southward for clarity. All the linear trends have passed the 95% confidence level.

while it migrates northward slightly from 1970 to 1992. After the early 1990s the mean position of the bifurcation shifts southward again with the same trend as in the first 20 years. However, we are not fully confident that the southward trend in the first two decades in SODA is real since there are no other available broad scale observations to guarantee the existence of its decadal transition. Although *Qiu and Chen* [2010] have shown in their Figure 7b that there existed a moderate southward shift before the 1970s, the trend is still too small compared with what we have shown based on SODA. Meanwhile, as indicated by *Qiu and Chen* [2010], NBL at the surface is positively correlated to the SSH in the key box (12°N–14°N, 127°E–130°E) and the southward/northward trend of the NBL can be explained by the rising/decreasing SSH in the box. But in *Merrifield* [2011], tide gauge records indicate that the recent high rates represent a significant increasing trend in the early 1990s relative to the preceding 40 years in the western tropical Pacific. Therefore, we would not find such a significant southward shift before the 1970s based on the relationship between SSH and NBL. This implies that the large southward shift of the NBL, as well as the upper layer transport in SODA, may be overestimated during the period 1950–1969. But we are sure that the southward trend of the bifurcation in the past two decades is significant, since it has solid observational support [*Qiu and Chen*, 2010, 2012].

[36] In addition to this newly developed SODA product, we assess other ocean reanalysis products including Simple Ocean Data Assimilation (SODA version 2.0.2/2.0.4), the German partner of the ECCO effort (GECCO) (see A. Köhl et al., The global ECCO 1952 to 2001 ocean synthesis, at http://www.ecco-group.org/pdfs/reports/report_40.pdf 2006) and ECMWF ORA-S3 ocean analysis/reanalysis system. Both of these NBLs derived from the multiple reanalysis products exhibit southward trends in the mean position, the same as we have shown in SODA 2.2.4 (Figure 13). Note that the multiple reanalysis products are independently forced by different wind stress data sets and the consistency among different products suggests a potential robustness of the southward shift of the NEC bifurcation in the Pacific Ocean and an important implication for the acceleration of the Kuroshio at its origin near the Philippine coast.

[37] Finally, we showed that the long-term change of the seasonal south–north migration of the NBL and its modulation by the long-term change of its mean position. Bifurcating of the NEC at a more southern latitude would make the upper ocean feel an increasing C_R, which plays a substantial role in determining its seasonal amplitude. Over the past six decades, C_R at the latitude of the bifurcation point increases from 13 cm s^{-1} in 1950 to 18 cm s^{-1} in 2005, and the corresponding A_b increases (decreases) before (after) the mid-1980s by about 0.5°. We find that A_b is very sensitive to C_R and it does not progressively increase along with the increasing C_R. Although A_b exhibits an amplifying trend, it can be expected from Figure 11b that A_b will decrease moderately in the following decades if the ocean continues warming, even if the mean position of the NBL does not shift. Changes in A_b may exert great impact on the seasonal variability of the Kuroshio at its origin and thus cause substantial changes in its intrusion into the South China Sea [e.g., *Metzger and Hurlburt*, 2001; *Xue et al.*, 2004; *Gan et al.*, 2006].

[38] **Acknowledgments.** This work is supported by the China National Science Foundation (NSFC) Major Research Project (40890150, 40890155) and NSFC Creative Group Project (40921004). We are very grateful to the two anonymous reviewers for their constructive comments. Discussions with Bo Qiu and Shantong Sun are greatly appreciated.

References

Balmaseda, M. A., A. Vidard, and D. L. T. Anderson (2008), The ECMWF Ocean Analysis System: ORA-S3, *Mon. Weather Rev.*, *136*, 3018–3034, doi:10.1175/2008MWR2433.1.

Cabanes, C., T. Huck, and A. C. D. Verdiere (2006), Contributions of wind forcing and surface heating to interannual sea level variations in the

Atlantic Ocean, *J. Phys. Oceanogr.*, *36*, 1739–1750, doi:10.1175/JPO2935.1.

Cai, W., G. Shi, T. Cowan, D. Bi, and J. Ribbe (2005), The response of the Southern Annular Mode, the East Australian Current, and the southern mid-latitude ocean circulation to global warming, *Geophys. Res. Lett.*, *32*, L23706, doi:10.1029/2005GL024701.

Carton, J. A., and B. S. Giese (2008), A reanalysis of ocean climate using Simple Ocean Data Assimilation (SODA), *Mon. Weather Rev.*, *136*, 2999–3017, doi:10.1175/2007MWR1978.1.

Chelton, D. B., R. A. de Szoeke, M. G. Schlax, K. E. Naggar, and N. Siwertz (1998), Geographical variability of the first baroclinic Rossby radius of deformation, *J. Phys. Oceanogr.*, *28*, 433–460, doi:10.1175/1520-0485(1998)028<0433:GVOTFB>2.0.CO;2.

Chen, Z., and L. Wu (2011), Dynamics of the seasonal variation of the North Equatorial Current bifurcation, *J. Geophys. Res.*, *116*, C02018, doi:10.1029/2010JC006664.

Compo, G. P., et al. (2011), The twentieth century reanalysis project, *Q. J. R. Meteorol. Soc.*, *137*, 1–28, doi:10.1002/qj.776.

Fine, R. A., R. Lukas, F. M. Bingham, M. J. Warner, and R. H. Gammon (1994), The western equatorial Pacific: A water mass crossroads, *J. Geophys. Res.*, *99*, 25,063–25,080, doi:10.1029/94JC02277.

Fu, L.-L., and B. Qiu (2002), Low-frequency variability of the North Pacific Ocean: The roles of boundary- and wind-driven baroclinic Rossby waves, *J. Geophys. Res.*, *107*(C12), 3220, doi:10.1029/2001JC001131.

Gan, J., H. Li, E. N. Curchitser, and D. B. Haidvogel (2006), Modeling South China Sea circulation: Response to seasonal forcing regimes, *J. Geophys. Res.*, *111*, C06034, doi:10.1029/2005JC003298.

Giese, B. S., and S. Ray (2011), El Niño variability in simple ocean data assimilation (SODA), 1871–2008, *J. Geophys. Res.*, *116*, C02024, doi:10.1029/2010JC006695.

Hazeleger, W. (2005), Can global warming affect tropical ocean heat transport?, *Geophys. Res. Lett.*, *32*, L22701, doi:10.1029/2005GL023450.

Jensen, T. G. (2011), Bifurcation of the Pacific North Equatorial Current in a wind-driven model: Response to climatological winds, *Ocean Dyn.*, *61*, 1329–1344, doi:10.1007/s10236-011-0427-2.

Kim, Y. Y., T. Qu, T. Jensen, T. Miyama, H. Mitsudera, H.-W. Kang, and A. Ishida (2004), Seasonal and interannual variations of the North Equatorial Current bifurcation in a high-resolution OGCM, *J. Geophys. Res.*, *109*, C03040, doi:10.1029/2003JC002013.

Kimura, S., T. Inoue, and T. Sugimoto (2001), Fluctuations in the distribution of low-salinity water in the North Equatorial Current and its effect on the larval transport of the Japanese eel, *Fish. Oceanogr.*, *10*, 51–60, doi:10.1046/j.1365-2419.2001.00159.x.

Liu, Z., S. G. H. Philander, and R. Pacanowski (1994), A GCM study of tropical-subtropical upper-ocean mass exchange, *J. Phys. Oceanogr.*, *24*, 2606–2623, doi:10.1175/1520-0485(1994)024<2606:AGSOTU>2.0.CO;2.

Lohmann, K., and M. Latif (2005), Tropical Pacific decadal variability and the subtropical-tropical cells, *J. Clim.*, *18*, 5163–5178, doi:10.1175/JCLI3559.1.

Lukas, R., E. Firing, P. Hacker, P. L. Richardson, C. A. Collins, R. Fine, and R. Gammon (1991), Observations of the Mindanao Current during the Western Equatorial Pacific Ocean Circulation Study, *J. Geophys. Res.*, *96*, 7089–7104, doi:10.1029/91JC00062.

McCreary, J. P., and P. Lu (1994), On the interaction between the subtropical and the equatorial oceans: The subtropical cell, *J. Phys. Oceanogr.*, *24*, 466–497.

Meehl, G. A., et al. (2007), The WCRP CMIP3 multi-model dataset: A new era in climate change research, *Bull. Am. Meteorol. Soc.*, *88*, 1383–1394, doi:10.1175/BAMS-88-9-1383.

Merrifield, M. A. (2011), A shift in western tropical Pacific sea level trends during the 1990s, *J. Clim.*, *24*, 4126–4138, doi:10.1175/2011JCLI3932.1.

Merryfield, W. J., and G. J. Boer (2005), Variability of upper Pacific Ocean overturning in a coupled climate model, *J. Clim.*, *18*, 666–683, doi:10.1175/JCLI-3282.1.

Metzger, E. J., and H. E. Hurlburt (2001), The nondeterministic nature of Kuroshio penetration and eddy shedding in the South China Sea, *J. Phys. Oceanogr.*, *31*, 1712–1732, doi:10.1175/1520-0485(2001)031<1712:TNNOKP>2.0.CO;2.

Nitani, H. (1972), Beginning of the Kuroshio, in *Kuroshio: Its Physical Aspects*, edited by H. Stommel and K. Yoshida, pp. 129–163, Univ. of Tokyo Press, Tokyo.

Pedlosky, J. (1996), *Ocean Circulation Theory*, 453 pp., Springer, New York.

Qiu, B., and S. Chen (2010), Interannual-to-decadal variability in the bifurcation of the North Equatorial Current off the Philippines, *J. Phys. Oceanogr.*, *40*, 2525–2538, doi:10.1175/2010JPO4462.1.

Qiu, B., and S. Chen (2012), Multi-decadal sea level and gyre circulation variability in the northwestern tropical Pacific Ocean, *J. Phys. Oceanogr.*, *42*, 193–206, doi:10.1175/JPO-D-11-061.1.

Qiu, B., and R. Lukas (1996), Seasonal and interannual variability of the North Equatorial Current, the Mindanao Current and the Kuroshio along the Pacific western boundary, *J. Geophys. Res.*, *101*, 12,315–12,330, doi:10.1029/95JC03204.

Qu, T., and R. Lukas (2003), The bifurcation of the North Equatorial Current in the Pacific, *J. Phys. Oceanogr.*, *33*, 5–18, doi:10.1175/1520-0485(2003)033<0005:TBOTNE>2.0.CO;2.

Rio, M.-H., P. Schaeffer, G. Moreaux, J.-M. Lemoine, and E. Bronner (2009), A new mean dynamic topography computed over the global ocean from GRACE data, altimetry and in-situ measurements, paper presented at the OceanObs'09 Symposium, Int. Oceanogr. Comm./UNESCO, Venice, Italy, 21–15 September.

Saenko, O. A., J. C. Fyfe, and M. H. England (2005), On the response of the oceanic wind-driven circulation to atmospheric CO_2 increase, *Clim. Dyn.*, *25*, 415–426, doi:10.1007/s00382-005-0032-5.

Sakamoto, T. T., H. Hasumi, M. Ishii, S. Emori, T. Suzuki, T. Nishimura, and A. Sumi (2005), Responses of the Kuroshio and the Kuroshio Extension to global warming in a high-resolution climate model, *Geophys. Res. Lett.*, *32*, L14617, doi:10.1029/2005GL023384.

Tokinaga, H., and S.-P. Xie (2011), Wave and Anemometer-based Sea-surface Wind (WASWind) for climate change analysis, *J. Clim.*, *24*, 267–285, doi:10.1175/2010JCLI3789.1.

Toole, J. M., R. C. Millard, Z. Wang, and S. Pu (1990), Observations of the Pacific North Equatorial Current bifurcation at the Philippine coast, *J. Phys. Oceanogr.*, *20*, 307–318, doi:10.1175/1520-0485(1990)020<0307:OOTPNE>2.0.CO;2.

Vecchi, G. A., B. J. Soden, A. T. Wittenberg, I. M. Held, A. Leetmaa, and M. J. Harrison (2006), Weakening of tropical Pacific atmospheric circulation due to anthropogenic forcing, *Nature*, *441*, 73–76, doi:10.1038/nature04744.

Wang, Q., and D. Hu (2006), Bifurcation of the North Equatorial Current derived from altimetry in the Pacific Ocean, *J. Hydrodynam.*, *18*(5), 620–626, doi:10.1016/S1001-6058(06)60144-3.

Wu, L., and C. Li (2007), Warming of the North Pacific Ocean: Local air-sea coupling and remote climatic impacts, *J. Clim.*, *20*, 2581–2601, doi:10.1175/JCLI4117.1.

Xue, H., F. Chai, N. Pettigrew, D. Xu, M. Shi, and J. Xu (2004), Kuroshio intrusion and the circulation in the South China Sea, *J. Geophys. Res.*, *109*, C02017, doi:10.1029/2002JC001724.